Development/Plasticity/Repair

Robo2 Drives Target-Selective Peripheral Nerve Regeneration in Response to Glia-Derived Signals

Patricia L. Murphy, Jesse Isaacman-Beck, and Michael Granato
Department of Cell and Developmental Biology, Perelman School of Medicine, University of Pennsylvania, Philadelphia, Pennsylvania 19104

Peripheral nerves are divided into multiple branches leading to divergent synaptic targets. This poses a remarkable challenge for regenerating axons as they select their original trajectory at nerve branch-points. Despite implications for functional regeneration, the molecular mechanisms underlying target selectivity are not well characterized. *Danio Rerio* (zebrafish) motor nerves are composed of a ventral and a dorsal branch that diverge at a choice-point, and we have previously shown that regenerating axons faithfully select their original branch and targets. Here we identify *robo2* as a key regulator of target-selective regeneration (sex of experimental subjects unknown). We demonstrate that *robo2* function in regenerating axons is required and sufficient to drive target-selective regeneration, and that *robo2* acts in response to glia located precisely where regenerating axons select the branch-specific trajectory to prevent and correct axonal errors. Combined, our results reveal a glia-derived mechanism that acts locally via axonal *robo2* to promote target-selective regeneration.

Key words: **collagen 4a5; peripheral nerve regeneration; *robo2*; schwann cells; target selection; zebrafish**

Significance Statement

Despite its relevance for functional recovery, the molecular mechanisms that direct regenerating peripheral nerve axons toward their original targets are not well defined. Zebrafish spinal motor nerves are composed of a dorsal and a ventral branch that diverge at a stereotyped nerve branch-point, providing a unique opportunity to decipher the molecular mechanisms critical for target-selective regeneration. Using a combination of live cell imaging and molecular-genetic manipulations, we demonstrate that the *robo2* guidance receptor is necessary and sufficient to promote target-selective regeneration. Moreover, we demonstrate that *robo2* is part of a genetic pathway that generates transient, spatially restricted, and tightly coordinated signaling events that direct axons of the dorsal nerve branch toward their original, pre-injury targets.

Introduction

The peripheral nervous system (PNS) has a remarkable capacity for axonal regeneration, and yet functional recovery from peripheral nerve injury is rare because axons regrow very slowly and often toward inappropriate targets. Supplementing pro-regenerative factors to regenerating PNS axons accelerates their growth rates yet falls short of providing spatial information to direct axons toward their original, pre-injury targets (Gordon and English, 2016). While components of many developmental axon guidance pathways are upregulated after nerve injury, their functional roles in directing regenerating axons are largely unknown (for review, see Giger et al., 2010). Thus, how regenerating axons navigate an environment that differs drastically from the embryo is not well understood.

In vertebrates, peripheral nerves exiting from the spinal cord divide repeatedly into progressively smaller branches, each carrying axons that innervate distinct synaptic targets (Lance-Jones and Landmesser, 1981). Depending on the type and location of a nerve injury, regenerating axons encounter a series of branch-points as they extend toward their original targets. For regenerating axons, repeatedly selecting the appropriate path at each branch-point, while critical to ensure functional regeneration, poses a formidable challenge. Although branch-specific regeneration of peripheral axons was first demonstrated >50 years ago (Mark, 1965; Politis, 1985), the molecular mechanisms that underlie branch-selective regeneration are largely unknown.

We previously established the optically transparent larval zebrafish as model to study the cellular and molecular mechanisms of target-selective peripheral nerve regeneration *in vivo* (Rosenberg et al., 2012). Zebrafish spinal motor nerves are composed of functionally distinct axonal populations that share a

Received July 27, 2021; revised Nov. 2, 2021; accepted Dec. 8, 2021.

Author contributions: M.G., P.L.M., and J.I.-B. designed research; M.G. and P.L.M. analyzed data; M.G. and P.L.M. edited the paper; P.L.M. and J.I.-B. performed research; P.L.M. wrote the first draft of the paper; P.L.M. wrote the paper.

This work was supported by National Eye Institute Grant EY024861 National Institute of Neurological Disorders and Stroke (NINDS) Grant 01NS097914 to M.G., and Eunice Kennedy Shriver National Institute of Child Health and Human Development (NICHD) GRANT T32HD083185 and National Institute of Neurological Disorders and Stroke (NINDS) GRANT 1F31NS103394 to P.L.M. We thank Daniel Morales, Leah Middleton, and Lauren Walker for technical assistance; and Dr. Andrea Stout (Penn Cell and Developmental Biology Microscopy Core and the Penn Sanger Sequencing Core) for technical support.

The authors declare no competing financial interests.

Correspondence should be addressed to Patricia L. Murphy at patti.murphy@gmail.com; Jesse Isaacman-Beck at jisaacmanbeck@gmail.com; or Michael Granato at granatom@pennmedicine.upenn.edu.

https://doi.org/10.1523/JNEUROSCI.1528-21.2021

common path before diverging into two major branches: a ventral nerve branch (see Fig. 1*A–E*, magenta) consisting of ~50 motor axons that innervate ventral muscles, and a dorsal nerve branch (see Fig. 1*A–E*, green) consisting of ~20 motor axons that innervate dorsal muscles (van Raamsdonk et al., 1983; Myers et al., 1986; Westerfield et al., 1986; Svara et al., 2018). Following dorsal nerve transection, the distal nerve undergoes Wallerian degeneration and is cleared away by macrophages, and the proximal nerve stump retracts into the spinal cord (see Fig. 1*C*). By 8 h post transection (hpt), the axons of the proximal stump regrow toward the nerve branch-point where they select their regenerative path (see Fig. 1*D*).

We have previously shown that regenerating spinal motor axons reliably choose the nerve branch that leads to their original muscle targets (Rosenberg et al., 2012). Live cell imaging revealed that regenerating axons of the dorsal nerve branch pause at the nerve branch-point, exploring both the incorrect ventral path and their original dorsal path before selecting the correct dorsal path. During this exploratory period, a small group of Schwann cells at the nerve branch-point simultaneously upregulate the extracellular matrix (ECM) component *col4a5* and the repulsive axon guidance cue *slit1a* (Isaacman-Beck et al., 2015), which bind each other with high affinity (Xiao et al., 2011). Moreover, we previously demonstrated that *col4a5* is required to guide regenerating dorsal axons, and proposed a model by which Schwann cell-derived Col4a5 scaffolds Slit at the nerve branch-point to prevent regenerating dorsal nerve branch axons from inappropriately entering into and extending along inappropriate trajectories (see Fig. 1*D*) (Isaacman-Beck et al., 2015).

To test this model, we used genetic mutants of the Slit-Robo signaling pathway. We find that the Slit-receptor *roundabout2* (*robo2*) and the Slit-Robo coreceptor heparan sulfate are dispensable for target-selective regeneration of ventral nerve axons, but required to direct regenerating dorsal nerve axons at the branch choice-point. Moreover, we find that *robo2* is expressed in dorsal nerve neurons, that expressing *robo2* in ventral nerve neurons is sufficient to redirect their regenerating axons into the dorsal nerve branch, and that this process requires *col4a5*. Finally, using live cell imaging, we demonstrate that during regeneration *robo2* functions at the nerve branch-point, preventing aberrant extension of dorsal nerve axons, thereby promoting growth toward their original, dorsal targets. Combined, our results reveal a previously unappreciated role for Slit-Robo signaling critical to ensure branch-selective and hence target-selective regeneration.

Materials and Methods

Fish lines and maintenance. All fish lines were maintained in Tügbingen or Tupfel longfin backgrounds as previously described (Mullins et al., 1994). We used the following mutant alleles, which were genotyped as previously described: *robo2-ti272z* (Fricke et al., 2001), *extl3-tm70g* (Lee et al., 2004), and *col4a5-s510* (Xiao and Baier, 2007). The *Tg(sox10:col4a5-myc)* line was generated as previously described (Isaacman-Beck et al., 2015) and genotyped by amplifying the Myc transgene using the following primers: 5′-GACTACAAGGATGACG ATGACAAG-3′ (forward) and 5′-TTCTCCCATAGTCACGCTAGC-3′ (reverse). For *in vivo* imaging, the following transgenic lines were used: $Tg(mnx1{:}GFP)^{ml3}$ (Flanagan-Steet et al., 2005) to visualize motor axons in both dorsal and ventral nerve branches, $Tg(isl1{:}GFP)^{rw0}$ (Uemura et al., 2005) to visualize dorsal nerve branch axons alone. Zebrafish veterinary care was performed under the supervision of the University Laboratory Animal Resources at the University of Pennsylvania. All zebrafish work was performed in accordance with protocols approved by the University of Pennsylvania Institutional Animal Care and Use.

Nerve transection. Dorsal and ventral nerves were transected using a nitrogen-pulsed dye (440 nm) laser as previously described (Rosenberg et al., 2012). Briefly, one of the two nerve branches (dorsal for Figs. 1-3, and 5 or ventral for Figs. 4, 6, and 7) was transected ~5 μm from the nerve branch-point (10-15 μm from the motor exit point [MEP]), leaving the other nerve branch intact and a ~5 μm gap between proximal and distal stumps of the transected nerve branch.

Before transection, larvae were genotyped by fin clipping at 3 d post fertilization (dpf) to ensure a mix of genotypes (~50% siblings and ~50% mutants) in each experiment. For this, caudal fins were resected using a microscalpel distal to the notochord and without breaching the caudal artery/vein loop. This method removes less tissue than published methods commonly performed before rearing larvae and is widely accepted not to affect gross development (Kosuta et al., 2018). After larvae were selected based on their genotypes, larvae were pooled and then randomly selected to blind the researcher to genotype during nerve transection. In $extl3^{-/-}$ larvae, dorsal nerves reach dorsal muscle targets, but a small subset grow along an aberrantly lateral trajectory. This phenotype is variably penetrant, affecting 0%-50% of nerves per larvae and <20% of all nerves across the mutant population ($n > 50$ larvae; P.L.M., unpublished observations). Thus, for dorsal nerve transections in progeny from $extl3^{+/-}$ parents, we carefully selected phenotypically normal nerves for transection.

Quantification of axon regeneration. Dorsal axon guidance before and after transection was quantified using modified Sholl analysis, as previously described (Isaacman-Beck et al., 2015), with the exception that line thickness in Sholl diagrams here does not correlate to fascicle thickness. When performing these analyses, nerves were deidentified and given unique IDs that could later be reassociated with their meta-data, so that researchers were blinded to genotype while scoring images. To calculate the regeneration error rate for each nerve, we divided the number of fascicles that regenerated outside the dorsal ROI ("errors") by the total number of fascicles that regenerated by 48 hpt. To determine the angle of ventral nerve extension, we measured the angle between two consistent points along the trunk of the nerve (50 and 100 μm from the MEP). The extent of ventral nerve regeneration was scored by counting the number of fascicles which regenerated at least 50 μm from the MEP by 48 hpt.

Immunohistochemistry and whole-mount FISH. To visualize *robo2* expression after nerve transection, dorsal nerves were transected in 5 dpf *Tg(isl1:GFP)* larvae. At 0-10 hpt, larvae were fixed in 4% PFA in PBS with 0.1% Tween-20 overnight at 4°C. Antisense *robo2* probe was synthesized from pBluescript-robo2 linearized with EcoRI using T3 RNA polymerase (Promega); sense *robo2* probe was synthesized from pBluescript-robo2 linearized with XhoI using T7 RNA polymerase (Promega). Probes were hydrolyzed in 0.6 M sodium carbonate and 0.4 M sodium bicarbonate at 60°C for 11 min to yield 300-500 bp fragments. Whole-mount ISH was performed as previously described (Thisse and Thisse, 2008) with the following modifications: 5 dpf larvae were permeabilized by digesting with Proteinase K (10 μg/ml, Promega) for 2 h; endogenous peroxidases were quenched by incubating in 0.3% H_2O_2 for 30 min before adding anti-digoxigenin antibody; for blocking and antibody incubation, we used 2% Blocking Reagent (Roche) in PBS with 0.1% Tween-20; probes were detected using sheep anti-digoxigenin POD Fab fragments (Roche) and developed for 2 min using Tyramide Signal Amplification (TSA Plus kit, PerkinElmer). We stained for *Tg(isl1:GFP)* using chicken anti-GFP (1:500, Aves Labs) detected by donkey anti-chick AlexaFluor-488 (1:500, Jackson ImmunoResearch Laboratories). Anti-digoxigenin POD and anti-GFP primary antibodies were incubated concurrently; secondary antibody was incubated at 4°C overnight after TSA.

Nerves were imaged using a 63× water immersion lens and 1 μm optical sections on a Carl Zeiss LSM 880 laser scanning confocal microscope and Zeiss Zen software or using a 40× water immersion lens and 1 μm optical sections on an Olympus Spinning disk confocal microscope and 3i Slidebook Software. Overlap between GFP antibody and *robo2* probe was quantified from 40× images in Fiji in the following way: motor pools of transected nerves were isolated by cropping optical sections in 3D; motor pools were then compressed into maximum intensity projections (MIPs); GFP and robo2 probe signals were separated and converted into binary masks using max entropy and moments methods, respectively; percent particle overlap between the two masks was calculated using the GDSC colocalization plugin; percent particle overlap was

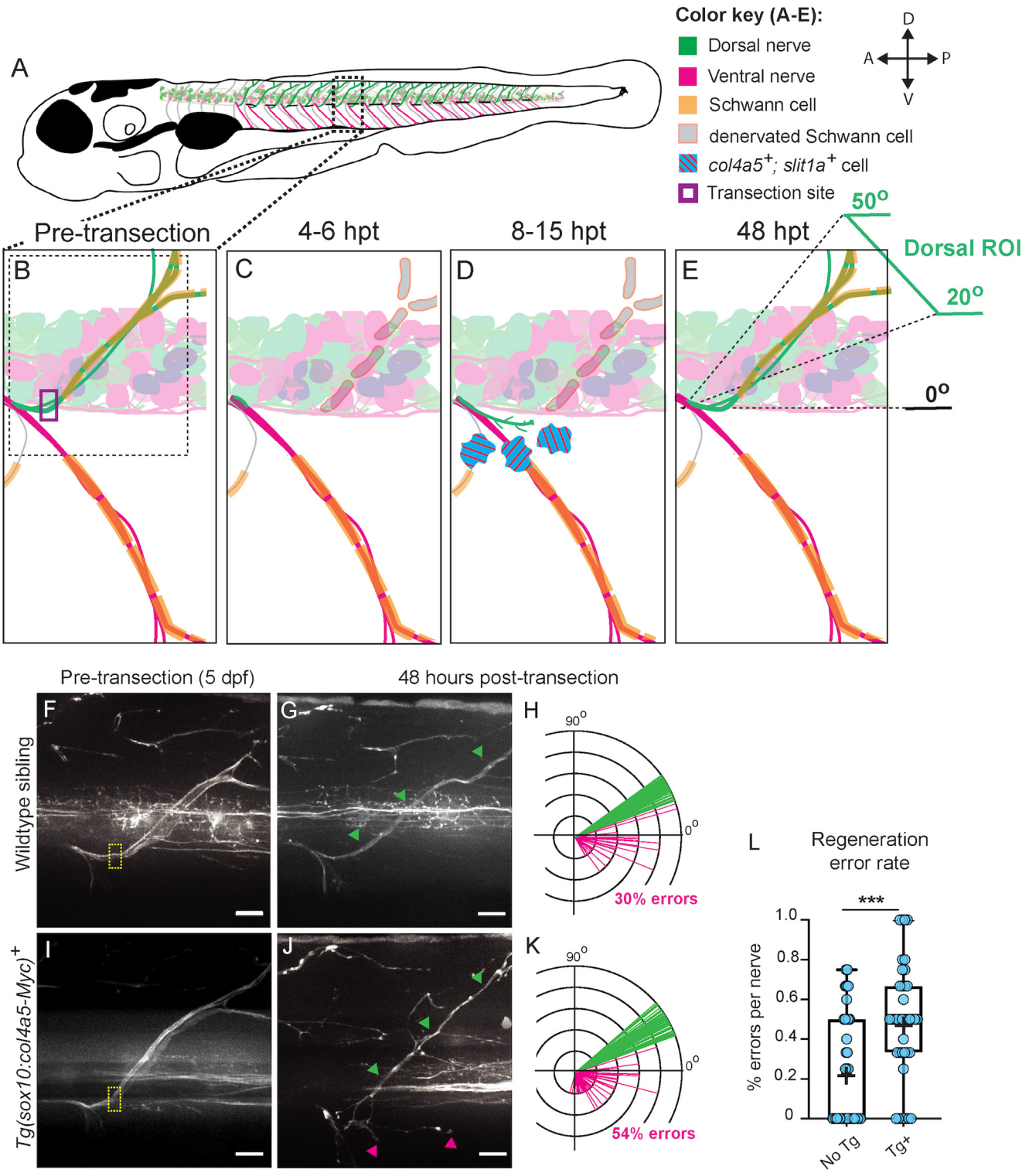

Figure 1. Spatiotemporal restriction of *col4a5* to the nerve branch-point is required for target-selective axon regeneration. Top, In 5 dpf larval zebrafish (schematized in ***A***), dorsal (green) and ventral (magenta) motor nerves exit the spinal cord in each body hemisegment via the ventral MEP and diverge at a stereotyped branch-point to innervate the dorsal and ventral muscles, respectively. ***B***, Magnified schematic of single motor nerve in dashed box in (***A***) pre-transection, showing dorsal (green) and ventral (magenta) branches of the spinal motor nerve and associated Schwann cells (orange). Purple box represents transection site. ***C***, By 4-6 hpt, the nerve distal to the transection site degenerates and is cleared away, and the proximal nerve retracts into the spinal cord. ***D***, At 8-15 hpt, growth cones enter the transection gap, and a small subset of Schwann cells at the nerve branch-point upregulate *col4a5* and *slit1a* (blue with red stripes). ***E***, By 48 hpt, the majority of dorsal axons regenerate into the dorsal ROI, defined as 20°-50° with respect to spinal cord. Bottom, Representative images of *Tg(isl1:GFP)*$^{+}$ dorsal nerves at 5 dpf and 48 hpt, respectively, in wild-type (WT) siblings (***F***,***G***) and *Tg(sox10:col4a5-myc)* larvae (***H***,***I***). Yellow boxes represent transection sites. Green arrowheads indicate dorsal regrowth. Magenta arrowheads indicate "errors" that regrew along nondorsal paths. Scale bars, 10 μm. Sholl diagrams showing overlay of all *Tg(isl1:GFP)* fascicle trajectories at 48 hpt in WT siblings (***G***, $n = 96$ fascicles) and *Tg(sox10:col4a5-myc)* larvae (***J***, $n = 133$ fascicles). For WT siblings, fascicles were counted for $n = 37$ nerves in 11 larvae; for *Tg(sox10:col4a5-myc)* larvae, fascicles were counted for $n = 40$ nerves in 11 larvae. Green lines indicate fascicles inside dorsal ROI. Magenta lines indicate fascicles outside of the dorsal ROI. Proportion of fascicles inside the dorsal ROI at 48 hpt was compared between *Tg(sox10:col4a5-myc)* larvae and WT siblings using one-tailed Fisher's exact test ($p = 0.0002$). ***K***, Graph of regeneration error rate for nerves in WT siblings (No Tg) and *Tg(sox10:col4a5-myc)* larvae (Tg^{+}) compared using one-tailed *t* test ($t_{(75)} = 3.807$, $p = 0.0001$). Each dot represents error rate for one nerve. +, Mean. ***$p < 0.001$.

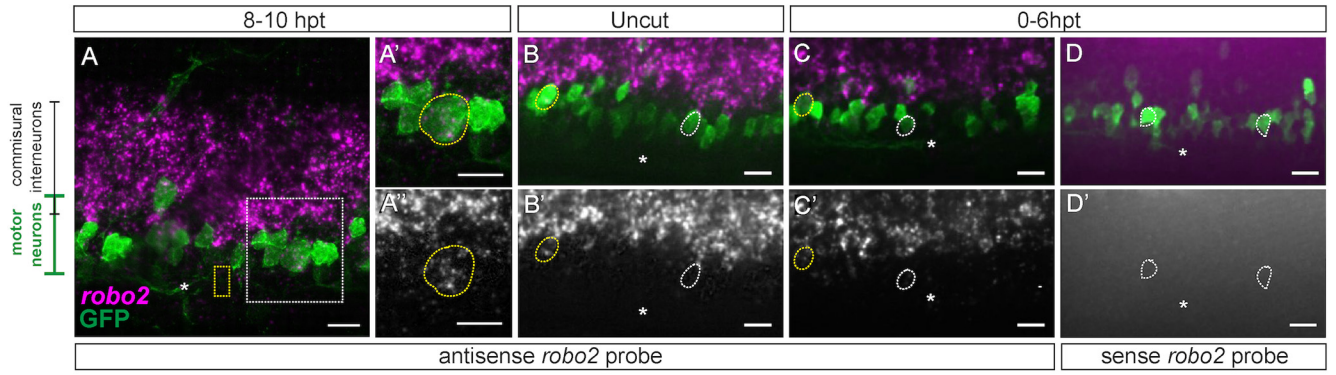

Figure 2. Robo2 is expressed in *isl1*$^+$ motor neurons before and after transection. ***A***, Representative image of *Tg(isl1:GFP)* motor neurons in spinal cord 8-10 hpt stained with *robo2* antisense ISH probe (magenta) and GFP antibody (green). Image shown is maximum *Z* projection of 24 optical sections (10 μm), 63×. Dashed yellow box represents transection site. Dashed white box represents area enlarged 1.5× in ***A′*** and ***A′′*** showing a single optical section (0.41 μm) with one *Tg(isl1:GFP)* motor neuron (green, outlined with yellow dashed line) expressing *robo2* mRNA (magenta) merged (***A′***) and alone (gray) (***A′′***). ***B–D***, Representative images of *Tg(isl1:GFP)* motor neurons stained with robo2 antisense ISH probe (***B***,***C***) or sense ISH probe control (***D***) (magenta) and GFP antibody (green) (merged). ***B′***, ***C′***, ISH probe of corresponding image alone (gray). Images shown are single optical sections (1 μm), 40× of nerves untransected (***B***) and at 0-6 hpt (***C***,***D***). White asterisks represent MEPs. Yellow dashed lines outline cell bodies with expression. White dashed lines outline cell bodies without expression. Scale bars, 10 μm.

then normalized across samples using the number of cell bodies manually counted in each motor pool.

Plasmid construction. The mnx1:mKate, mnx1:robo2 plasmid was constructed using Gateway cloning (Kwan et al., 2007) using pME:robo2 (Campbell et al., 2007) and pI-SceI mnx1:mKate, mnx1:DEST, which encodes two mnx1 promoters in tandem (Bremer and Granato, 2016), to insert the *robo2* coding sequence behind the second mnx1 promoter. To construct plasmid for synthesis of *robo2 in situ* probe (pBluescript-robo2), the full-length *robo2* coding sequence was amplified from the mnx1:mKate, mnx1:robo2 plasmid using the following primers 5′-AGTCAGCTC GAGAACGTGTTCTGGGGTTGAGA-3′ (forward, includes XhoI restriction site) and 5'GCTAACGAATTCTGGGTATGAGGCATTTCCAGA AC-3′ (reverse, includes EcoRI restriction site). XhoI and EcoRI restriction sites were used to clone this product into pBluescript II KS+.

Sparse axonal labeling. We used mnx1:mKate, mnx1:robo2 and mnx1:mKate, mnx1:mKate to label small numbers of ventral motor neurons by injecting 50-100 pg of plasmid DNA into one-cell stage embryos with Isce-I, as previously described (Downes et al., 2002). We have previously validated that both mnx1 promoters in this construct are active and drive comparable levels of expression (Bremer and Granato, 2016). At 3 dpf, injected larvae with mKate expression were screened for ventral nerves with very few labeled axons using a 40× water immersion lens on Olympus spinning disk confocal microscope using 3i Slidebook software. When examining branch-specific labeling in development and regeneration, larvae and nerves were deidentified and given unique IDs that could later be reassociated with their meta-data, so that researchers were blinded to the injection condition and genotype while scoring. Nerves were scored as "dorsal" if any mKate$^+$ fascicles were present along the dorsal branch, regardless of whether mKate$^+$ fascicles were also present along the ventral branch.

It was technically challenging to sparsely label ventral axons in sufficient numbers for transection experiments without labeling multiple neurons per motor pool. We could almost always count multiple (2-6) mKate$^+$ cell bodies in motor pools corresponding to transected ventral nerves (data not shown). After ventral nerve transection, we often observed that *Tg(mnx1:mKate;mnx1:robo2)*$^+$ fascicles regenerated along both the dorsal and the ventral branch (see Fig. 6*D*). While we cannot exclude the possibility that these samples represent single bifurcating axons, we believe it is very likely that this reflects the regeneration of multiple labeled axons. Therefore, at 48 hpt, we scored mKate$^+$ fascicle regeneration as "ventral" if mKate$^+$ fascicles were observed only on the ventral nerve branch, and we scored mKate$^+$ fascicle regeneration as "dorsal" if we observed any mKate$^+$ along the dorsal branch, regardless of whether mKate$^+$ fascicles were also present along the ventral branch.

Live imaging. Larvae were anesthetized, mounted in agarose, and imaged on a spinning disk confocal microscope as previously described (Rosenberg et al., 2012). We began our time-lapse experiments at 7-9 hpt and filmed regeneration for 12-15 h. Because of variability in time when axons started regrowing (8-14 hpt), we quantified axon dynamics starting when the first regenerating fascicle reached the nerve branch-point, ending up to 10 h later. We analyzed regenerating fascicles for a total of 5940 min in siblings ($n = 9$ nerves) and 5030 min in mutants ($n = 10$ nerves). When analyzing regeneration dynamics, nerves were deidentified and given unique IDs that could later be reassociated with their meta-data, so that researchers were blinded to genotype while scoring.

Image processing. For ventral nerves (see Fig. 4) and fixed samples (see Fig. 2), *Z* stacks were compressed into MIPs. Brightness and contrast were automatically optimized based on the image histogram in Fiji ImageJ (National Institutes of Health). The dorsal nerve branch wraps around the spinal cord, closely apposed to motor neuron cell bodies, which are labeled brightly by our transgenic lines. To visualize the dorsal nerves independently of neuron cell bodies (see Figs. 1, 3, 5-7), we used Fiji to create multiple MIPs from the same *Z* stack, including only optical sections that contained the dorsal nerve without neuron cell bodies in each *XY* position. These MIPs were adjusted to equivalent brightness and contrast and then stitched together using the Pairwise Stitching plugin (Preibisch et al., 2009).

Experimental design and statistical analysis. For all experiments, desired sample sizes were defined before beginning data collection. For dorsal nerve transection and live imaging experiments, we determined appropriate sample sizes based on those in previously published experiments that were able to detect effects of the sizes that we expected. For stochastic labeling experiments, sample sizes were determined via power analyses using G*Power (Faul et al., 2007). Zebrafish sex determination is polygenic and at the larval stage (28 dpf or earlier) requires multiple qPCRs that have only recently been identified (King et al., 2020). Therefore, we were unable to control for the sex of our experimental subjects.

Continuous data (see Fig. 5) were analyzed using one- or two-tailed *t* tests, as dictated by experimental design and indicated in the figure legends. Categorical data (see Figs. 1, 3, 6, 7) were analyzed in contingency tables using one- or two-tailed Fisher's exact tests for proportionality, as indicated in the figure legends. Count data (see Fig. 5) were analyzed using two-tailed Mann–Whitney tests.

Results

Col4a5 upregulation at the nerve branch-point is critical to guide regenerating dorsal axons

We previously demonstrated that the glycosyltransferase *lysyl-hydrosylase-3* (*lh3*) and its substrate *collagen-4-α-5* (*col4a5*) are required to direct regenerating dorsal nerve axons toward their

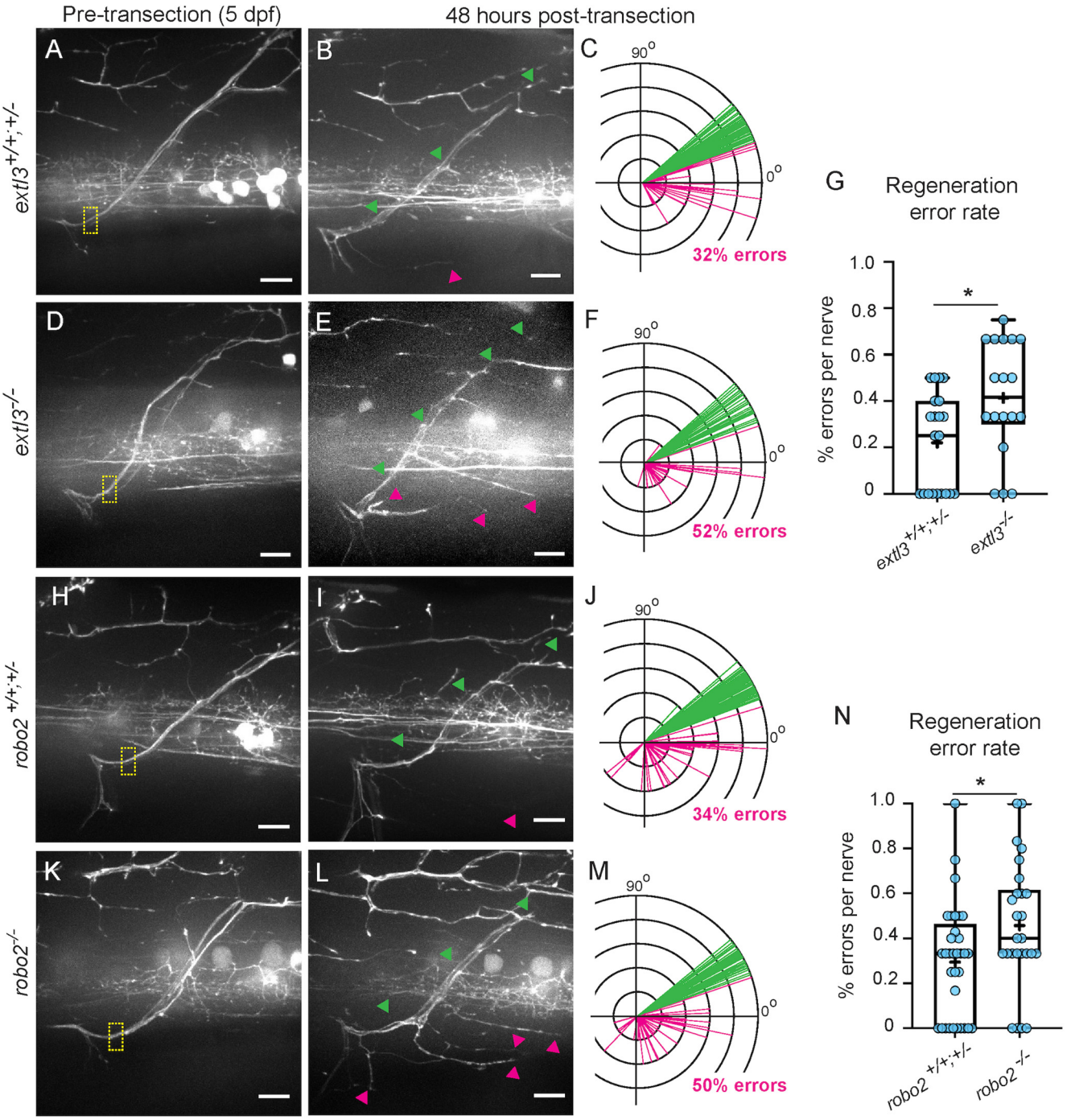

Figure 3. Slit-Robo signaling is required to guide regenerating dorsal nerve branch axons. Representative images of dorsal nerves in *extl3* WT siblings at 5 dpf and 48 hpt, respectively, in *extl3* WT siblings (***A***,***B***), $extl3^{-/-}$ (***D***,***E***), *robo2* WT siblings (***H***,***I***), and $robo2^{-/-}$ (***K***,***L***). Yellow boxes represent transection sites. Green arrowheads indicate dorsal regrowth. Magenta arrowheads indicate "errors" that regrew along ventral and ventrolateral paths. Scale bars, 10 μm. Sholl diagrams showing overlay of all *Tg(isl1:GFP)* fascicle trajectories at 48 hpt in *extl3* WT siblings (***C***, $n = 98$ fascicles), $extl3^{-/-}$ (***F***, $n = 58$ fascicles), *robo2* WT siblings (***J***, $n = 108$ fascicles), and $robo2^{-/-}$ (***M***, $n = 97$ fascicles). Green lines indicate fascicles inside dorsal ROI. Magenta lines indicate fascicles outside of the dorsal ROI. For *extl3* WT siblings, fascicles were counted in $n = 38$ nerves in 19 larvae; for $extl3^{-/-}$ larvae, fascicles were counted in $n = 23$ nerves in 7 larvae; for *robo2* WT siblings, fascicles were counted in $n = 33$ nerves in 16 larvae; for $robo2^{-/-}$ larvae, fascicles were counted in $n = 26$ nerves in 9 larvae. Proportion of fascicles inside the dorsal ROI at 48 hpt was compared using one-tailed Fisher's exact test between *extl3* WT siblings and $extl3^{-/-}$ larvae ($p = 0.0105$) and *robo2* WT siblings and $robo2^{-/-}$ larvae ($p = 0.0134$). ***G***, Graph of regeneration error rate for nerves in *extl3* WT siblings and $extl3^{-/-}$ larvae compared using one-tailed *t* test ($t_{(53)} = 2.862$, $p = 0.003$). ***N***, Graph of regeneration error rate for nerves in *robo2* WT siblings and $robo2^{-/-}$ larvae compared using one-tailed *t* test ($t_{(57)} = 2.333$, $p = 0.0116$). Each dot represents error rate for one nerve. *$p < 0.05$.

original targets (Isaacman-Beck et al., 2015). *Lh3* is constitutively expressed at low levels and acts in Schwann cells to promote target-selective regeneration, while *col4a5* expression is transiently upregulated 8-15 hpt in a small subset of Schwann cells near the nerve branch-point (Fig. 1*D*) (Isaacman-Beck et al., 2015), suggesting that *col4a5* expression restricted to the nerve branch-point might be instructive in directing regenerating axons. To test this idea, we generated a transgenic line, *Tg(sox10:col4a5-Myc)*, in which *col4a5* is now expressed in all Schwann cells, before and following peripheral nerve transection (Isaacman-

Beck et al., 2015). Before nerve transection, dorsal nerves in wild-type (WT) siblings appear indistinguishable from those in transgenic animals expressing *col4a5* in all Schwann cells (compare Fig. 1*F* with Fig. 1*I*). Specifically, we quantified targeting of *Tg(isl1:GFP)*$^{+}$ dorsal nerve axons before nerve transection in 5-d-old animals. Dorsal nerve axons tightly fasciculate with one another, precluding us from quantifying individual axons contained in *Tg(isl1:GFP)*$^{+}$ dorsal nerves. We therefore quantified the number of discernable *Tg(isl1:GFP)*$^{+}$ fascicles and determined the fraction of fascicles within the dorsal muscle target area, which we previously defined as spanning 30 deg before transection (dorsal ROI in Fig. 1*E*) (Isaacman-Beck et al., 2015). When we compared these fractions across genotypes, we found no significant difference in dorsal fascicles between *Tg(sox10:col4a5-Myc)* animals and WT siblings ($n = 103$ of 105 fascicles in in dorsal ROI WT siblings, $n = 99$ of 101 in *Tg(sox10:col4a5-Myc)* larvae; $p = 0.6746$, one-tailed Fisher's exact test), suggesting that, in *Tg(sox10:col4a5-Myc)* animals, dorsal nerve targeting during development is unaffected.

To determine whether spatially restricted expression of *col4a5* is critical for target-selective regeneration, we laser-transected dorsal nerves in WT and *Tg(sox10:col4a5-Myc)* larvae and compared target-selective regeneration at 48 hpt, when WT motor axons have reestablished functional connections with their muscle targets (Rosenberg et al., 2012). In WT animals, 70% of fascicles containing dorsal nerve axons regenerated to their original dorsal target area (Fig. 1*G*,*H*; 96 fascicles, 37 nerves, 11 larvae), consistent with previous findings that regenerating axons readily select their original branch and targets (Isaacman-Beck et al., 2015). In contrast, transgenic expression of *col4a5* in all Schwann cells reduced target-selective regeneration significantly. In *Tg(sox10:col4a5-myc)*-expressing larvae, only 46% of the fascicles containing dorsal nerve axons selected their original dorsal trajectory (133 fascicles, 40 nerves, 11 larvae), concomitant with an 1.8-fold increase from 30% to 54% fascicles selecting incorrect ventral and lateral trajectories (Fig. 1*J*,*K*; $p = 0.0002$, one-tailed Fisher's exact test). We next examined the regeneration error rate for individual nerves at 48 hpt and found that, compared with WT siblings, nerves in *Tg(sox10:col4a5-myc)*-expressing larvae displayed errors at a significantly higher rate (Fig. 1*L*; $t_{(75)} = 3.807$, $p = 0.0001$, one-tailed *t* test). Thus, expanding *col4a5* expression from a small subset of Schwann cells strategically positioned at the nerve branch region to all Schwann cells impairs target-selective regeneration. Moreover, the resulting phenotype closely mirrors the phenotype in mutants lacking *col4a5* (Isaacman-Beck et al., 2015). These results support the idea that *col4a5*'s transient expression in a subset of Schwann cells at the nerve branch-point where regenerating axons of the dorsal branch select their branch specific trajectory is of functional importance.

Slit-Robo signaling is required for target-selective regeneration

The same small group of Schwann cells that upregulates *col4a5* after injury concurrently upregulates *slit1a* (Isaacman-Beck et al., 2015), suggesting that, similar to *col4a5*, *slit1a* might play a functional role in target-selective regeneration. *Slit1a* encodes a canonical ligand for the Roundabout (Robo) family of repulsive axon guidance receptors (Blockus and Chédotal, 2016) and is the only one of the four Slit ligands whose injury-induced expression mirrors that of *col4a5* (Isaacman-Beck et al., 2015). Moreover, in the developing zebrafish visual system, Col4a5 directly binds to, and is required for, basement membrane anchoring of Slit, which guides laminar targeting of retinal ganglion cell axons through *robo2* (Xiao et al., 2011). We therefore wondered whether *robo2* is involved in guiding regenerating dorsal axons. Using whole-mount FISH, we detected *robo2* mRNA expression in *Tg(isl1:GFP)*$^{+}$ motor neurons of the dorsal nerve before transection and also during regeneration (Fig. 2*A*–*C*, uncut: $n = 65$ nerves, 1220 motor neurons uncut; 0-4 hpt: $n = 28$ nerves, 499 motor neurons; 4-6 hpt: $n = 16$ nerves, 365 motor neurons; 6-10 hpt: $n = 22$ nerves, 469 motor neurons).

We next asked whether Slit-Robo signaling plays a functional role in target-selective regeneration. For this, we examined dorsal nerve regeneration in genetic mutants for two Slit-Robo signaling components: *exotosin-like-3* (*extl3*), a glycosyltransferase required for the biosynthesis of heparan sulfate proteoglycans, which are critical to stabilize Slit-Robo binding (Hussain et al., 2006); and the Robo-receptor *robo2*. We first examined dorsal nerve regeneration in *extl3* mutants, which at 5 dpf lack detectable levels of heparan sulfate (Lee et al., 2004). Before nerve transection, targeting of dorsal nerve axons in 5 dpf *extl3* mutants was indistinguishable from their siblings (compare Fig. 3*A*–*D*; $n = 103$ of 108 fascicles in dorsal ROI in *extl3*$^{+/+;+/-}$, $n = 43$ of 44 in *extl3*$^{-/-}$, $p = 0.4399$, one-tailed Fisher's exact test). In WT siblings, 68% of regenerating dorsal nerve fascicles returned to their original, dorsal targets (Fig. 3*B*,*C*), while 32% selected ventral and ventrolateral trajectories (38 nerves from 19 larvae). In contrast, in *extl3* mutants, we observed a 1.6-fold increase (from 32% to 52%) of dorsal nerve fascicles failing to select their dorsal trajectory, instead extending along erroneous ventral or ventrolateral trajectories (23 nerves from 7 larvae) (Fig. 3*E*,*F*; $p = 0.0105$, one-tailed Fisher's exact test). Similarly, compared with WT siblings, individual nerves in *extl3* mutants formed errors at a significantly higher rate at 48 hpt (Fig. 3*G*; $t_{(53)} = 2.862$, $p = 0.003$, one-tailed *t* test).

We next examined the role of Robo2 in dorsal nerve regeneration. Before transection, dorsal nerve targeting in *robo2* mutant animals was slightly lower than what we observed in *robo2* WT siblings (compare Fig. 3*H*–*K*; $n = 103$ of 108 fascicles in dorsal ROI in *robo2*$^{+/+;+/-}$, $n = 67/79$ in *robo2*$^{-/-}$, $p = 0.0548$, one-tailed Fisher's exact test), yet still within the range we have previously observed in WT animals (Isaacman-Beck et al., 2015). Following nerve transection in WT siblings, 34% of dorsal nerve fascicles failed to select their original trajectory, while the vast majority returned to their original target area (66%; Fig. 3*I*,*J*). In contrast, in *robo2* mutants only 50% of regenerating dorsal nerve fascicles returned to their original target area, an almost 1.5-fold increase of *Tg(isl1:GFP)*$^{+}$ fascicles now extending along aberrant ventral or ventrolateral trajectories (Fig. 3*L*,*M*; $p = 0.0134$, Fisher's exact test). Similarly, compared with nerves in WT siblings at 48 hpt, individual nerves in *robo2* mutants exhibited significantly higher error rates (Fig. 3*N*; $t_{(57)} = 2.333$, $p = 0.0116$, one-tailed *t* test). Together, these results demonstrate that Slit-Robo signaling plays a functional role in directing regenerating dorsal nerve axons along their original, pre-injury trajectories. Finally, to determine whether *extl3* and *robo2* play a selective role in promoting target selection of dorsal, rather than ventral, nerve axons, we transected ventral nerves in *extl3* and *robo2* mutants. At 5 dpf and 48 hpt, ventral nerves in *extl3* and *robo2* mutants are indistinguishable from their siblings (Fig. 4*A*–*J*). Similarly, compared with their siblings, we found no significant difference in the number (Fig. 4*E*,*K*) or angle of extension (Fig. 4*F*,*L*) of ventral nerve fascicles in *robo2* or *extl3* mutants before or after injury. Together, these results demonstrate that Slit-Robo signaling is selectively required for dorsal nerve target-selective regeneration.

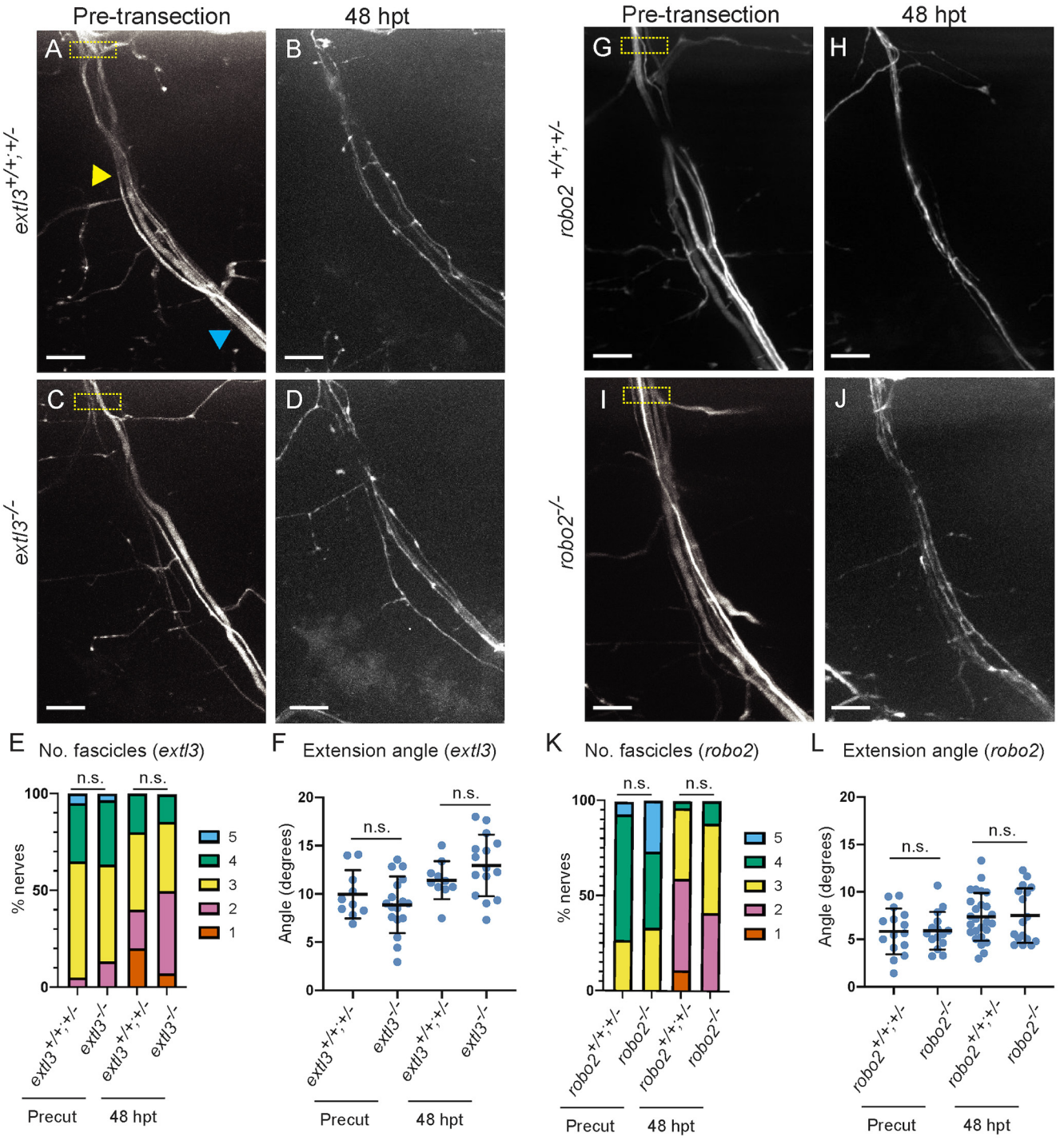

Figure 4. Slit-Robo signaling is dispensable for ventral nerve branch development and regeneration. Top, Representative images of *Tg(hb9:GFP)* ventral nerves at 5 dpf and 48 hpt, respectively, in *extl3* siblings (***A***,***B***), *extl3*$^{-/-}$ (***C***,***D***), *robo2* WT siblings (***G***,***H***), and *robo2*$^{-/-}$ (***I***,***J***). MEP is just dorsal to the top of imaging frame shown. ***A***, Arrowheads indicate 50 μm (yellow arrowhead) and 100 μm (blue arrowhead) from the MEP. Dashed yellow boxes represent transection site (10-15 μm ventral to MEP). Bottom, Quantification of ventral nerve fascicles at 5 dpf (Precut) and 48 hpt in (***E***) *extl3* WT siblings ($n = 20$ nerves, 11 larvae) and *extl3*$^{-/-}$ larvae ($n = 30$ nerves, 16 larvae) and (***K***) *robo2* WT siblings ($n = 10$ nerves, 5 larvae) and *robo2*$^{-/-}$ larvae ($n = 17$ nerves, 9 larvae). Nerves were scored by counting the number of discrete fascicles discernible 50 μm from the MEP (***A***, yellow arrowhead). Genotypes were compared using two-tailed *t* tests (for *extl3*: Precut, $p = 0.6875$; 48 hpt, $p = 0.9167$ for *robo2*: Precut $p = 0.6009$; 48 hpt, $p = 0.1003$). Angle of ventral nerve extension at 5 dpf and 48 hpt in (***F***) *extl3* WT siblings ($n = 10$ nerves, 5 larvae) and *extl3*$^{-/-}$ larvae ($n = 17$ nerves, 9 larvae) and (***L***) *robo2* siblings ($n = 26$ nerves, 10 larvae) and *robo2*$^{-/-}$ larvae ($n = 17$ nerves, 7 larvae). Extension angle was calculated as the difference between the angle of the nerve between 50 μm from the MEP (***A***, yellow arrowhead) and 100 μm from MEP (***A***, blue arrowhead). Each dot represents one nerve. Genotypes were compared using two-tailed *t* tests (for *extl3*: Precut, $p = 0.3403$; 48 hpt, $p = 0.1900$; for *robo2*: Precut $p = 0.9424$; 48 hpt, $p = 0.8731$).

Robo2 promotes target-selective regeneration at the nerve branch-point by preventing and correcting errors

To further understand the cellular mechanisms by which *robo2* promotes target-selective regeneration, we examined the dynamics of regenerating axons navigating the nerve branch-point in *robo2* mutants. We have previously shown that, after dorsal nerve transection in WT larvae, regenerating axons pause at the nerve branch-point and extend growth cones toward their original dorsal targets,

as well as along erroneous ventral and lateral trajectories. Over the next few hours, erroneous projections are destabilized, while growth cones along the dorsal path stabilize and continue to extend toward their original targets (Isaacman-Beck et al., 2015). To determine whether *robo2* directs regenerating dorsal nerve axons early in the process by minimizing the formation of erroneous projections, or subsequently by destabilizing already extending erroneous projections, we performed time-lapse imaging between 8 and 20 hpt as regenerating *robo2* mutant dorsal nerve axons navigate the branch choice-point (Fig. 5*A–H*; Movies 1 and 2). From these movies, we quantified the number of erroneous projections (errors), defined as *Tg(isl1:GFP)*$^{+}$ growth $\geq$1 μm that extended from the nerve branch-point along erroneous ventral or lateral trajectories (for more details, see Materials and Methods). Compared with WT siblings, *robo2* mutants exhibit no significant difference in the number of errors that form at the branch-point (Fig. 5*I*), suggesting that *robo2*-does not play a role in error formation, whether it occurs by collateral sprouting or other mechanisms. To determine whether there was a deficit in error correction at the branch-point in *robo2* mutants, we counted the number of errors (Fig. 5*A–H*, magenta arrowheads; Movies 1 and 2) that were corrected. Errors were counted as "corrected" if they retracted within <1 μm away from the nerve branch-point. Compared with siblings, *robo2* mutants displayed a significant decrease in the percent of errors that were corrected during early regeneration (Fig. 5*J*).

Based on the well-characterized role of Slit-Robo in axon repulsion (Blockus and Chédotal, 2016), we considered whether in *robo2* mutants the deficit in error correction at the nerve branch-point might be because of reduced error retraction. To test this, we measured in WT siblings and *robo2* mutants the percent of time that errors spent retracting, extending, or being stable (no movement). We failed to detect any significant difference in relative time that errors spent retracting in *robo2* mutants compared with WT siblings (Fig. 5*K*). Similarly, we did not observe any differences in the average speed of extension or retraction in *robo2* mutants compared with siblings (Fig. 5*L*). Instead, compared with WT siblings, erroneous projections (errors) in *robo2* mutants spent significantly more time extending (Fig. 5*K*). This is the result of a combined reduction in the time that errors spent retracting and stable in *robo2* mutants, neither of which is statistically significant on its own (Fig. 5*K*). These results suggest that, rather than promoting axonal retraction along incorrect trajectories, *robo2* promotes dorsal nerve target selection by preventing axon extension along erroneous ventral and lateral trajectories. Consistent with this idea, compared with WT siblings, erroneous projections in *robo2* mutants grew longer distances (Fig. 5*M*). Combined with previous results this provides strong support for a model in which *robo2* expression on regenerating dorsal nerve axons prevents and corrects errors at the nerve branch-point in response to Slit1a transiently produced by a small subset of adjacent Schwann cells and spatially scaffolded by Col4a5. By preventing error extensions, *robo2* tilts the balance between extension and retraction such that errors retract more often than they extend. This results in shorter errors that are readily corrected through *robo2*-independent mechanisms of retraction, ultimately biasing regenerating dorsal nerve axons toward their original dorsal trajectory.

Robo2 expression drives target-selective regeneration

We next asked how Slit-Robo signaling selectively influences regeneration of dorsal, but not ventral, nerve axons. One possibility is that *robo2* functions selectively in dorsal nerve axons, enabling regenerating axons of only the dorsal, but not the ventral, branch to mount a *slit1a*-dependent error response at the nerve branch-point. We hypothesized that, if this were the case, forcing *robo2* expression in regenerating ventral nerve axons would redirect them onto a dorsal trajectory. To test whether *robo2* expression is indeed sufficient to drive target-selective regeneration, we used the motor neuron-specific mnx1 promotor (Flanagan-Steet et al., 2005) to transiently express mKate alone or mKate with *robo2* in small subsets of motor neurons (for more details, see Materials and Methods). Importantly, compared with mKate expression, *robo2*-mKate expression in motor neurons did not affect their developmental bias in selecting a ventral or dorsal trajectory (for *Tg(mnx1:mKate; mnx1:mKate)*, $n = 23$ of 41 nerves contained at least one visible mKate^{+} fascicle within the dorsal ROI at 5 dpf; for *Tg(mnx1:mKate; mnx1:robo2)*, $n = 22$ of 41 nerves; $p = 0.9999$, Fisher's exact test) nor did it impair their ability to regrow an axon (for *Tg(mnx1:mKate; mnx1:mKate)*, $n = 13$ of 26 nerves regenerated by 48 hpt; for *Tg(mnx1:mKate; mnx1:robo2)*, $n = 15$ of 32 nerves; $p = 0.999$, Fisher's exact test). This is consistent with the absence of a developmental motor axon phenotype in *robo2* mutants, further confirming that *robo2* acts selectivity during the regeneration process. To determine whether *robo2* is sufficient to promote dorsal branch selection in regenerating axons, we screened for spinal motor nerves with small subsets of mKate^{+} axons along the ventral, but not the dorsal, branch (Fig. 6*A*,*C*). We laser-transected these ventral nerves and assessed the regeneration of mKate^{+} fascicles at 48 hpt. We found that regenerating mKate^{+} ventral nerve axons always selected a ventral path toward their original targets (Fig. 6*B*), consistent with previous results (Rosenberg et al., 2012). In contrast, forcing *robo2*-mKate expression in regenerating ventral nerve axons was sufficient to redirect them onto a dorsal trajectory (Fig. 6*C*,*D*; Fisher's exact test $p = 0.0069$). Importantly, the trajectories taken by these axons were indistinguishable from those taken endogenously by dorsal nerve axons (compare with Fig. 3*B*,*I*). Thus, *robo2* is both required and sufficient to drive target-selective regeneration.

Robo2 requires *col4a5* function for target-selective regeneration

In *robo2* and *col4a5* mutants, ventral branch axons reliably regenerate along their appropriate ventral path (Fig. 4) (Isaacman-Beck et al., 2015), while dorsal branch axons frequently fail to select their original dorsal trajectory and instead extend along erroneous, ventral and lateral trajectories. Because of the similarities of their mutant phenotypes, we next asked whether *robo2* and *col4a5* act through two distinct pathways or whether they are both part of one common pathway. We reasoned that, if the latter was the case, then redirecting ventral nerve axons toward dorsal trajectories via forced *robo2* expression should depend on *col4a5* function. To test this hypothesis, we repeated the *robo2* mis-expression experiment driving sparse expression of either mKate or *robo2*-mKate in small subsets of regenerating ventral nerve axons, but now in a *col4a5* mutant background. Before nerve transection at 5 dpf, there was no difference between the branch-selection of sparsely labeled WT and *robo2*-expressing axons in *col4a5* siblings or mutants (for *col4a5*$^{+/+;+/-}$: *Tg(mnx1:mKate; mnx1:mKate)*, $n = 39$ of 89 nerves contained at least one visible mKate^{+} fascicle within the dorsal ROI at 5 dpf; *Tg(mnx1:mKate; mnx1:robo2)*, $n = 42$ of 80 nerves, $p = 0.2831$, Fisher's exact test; for *col4a5*$^{-/-}$ larvae: *Tg(mnx1:mKate; mnx1:mKate)*, $n = 33$ of 48 nerves; *Tg(mnx1:mKate; mnx1:robo2)*, $n = 13$ of 26 nerves, $p = 0.1364$, Fisher's

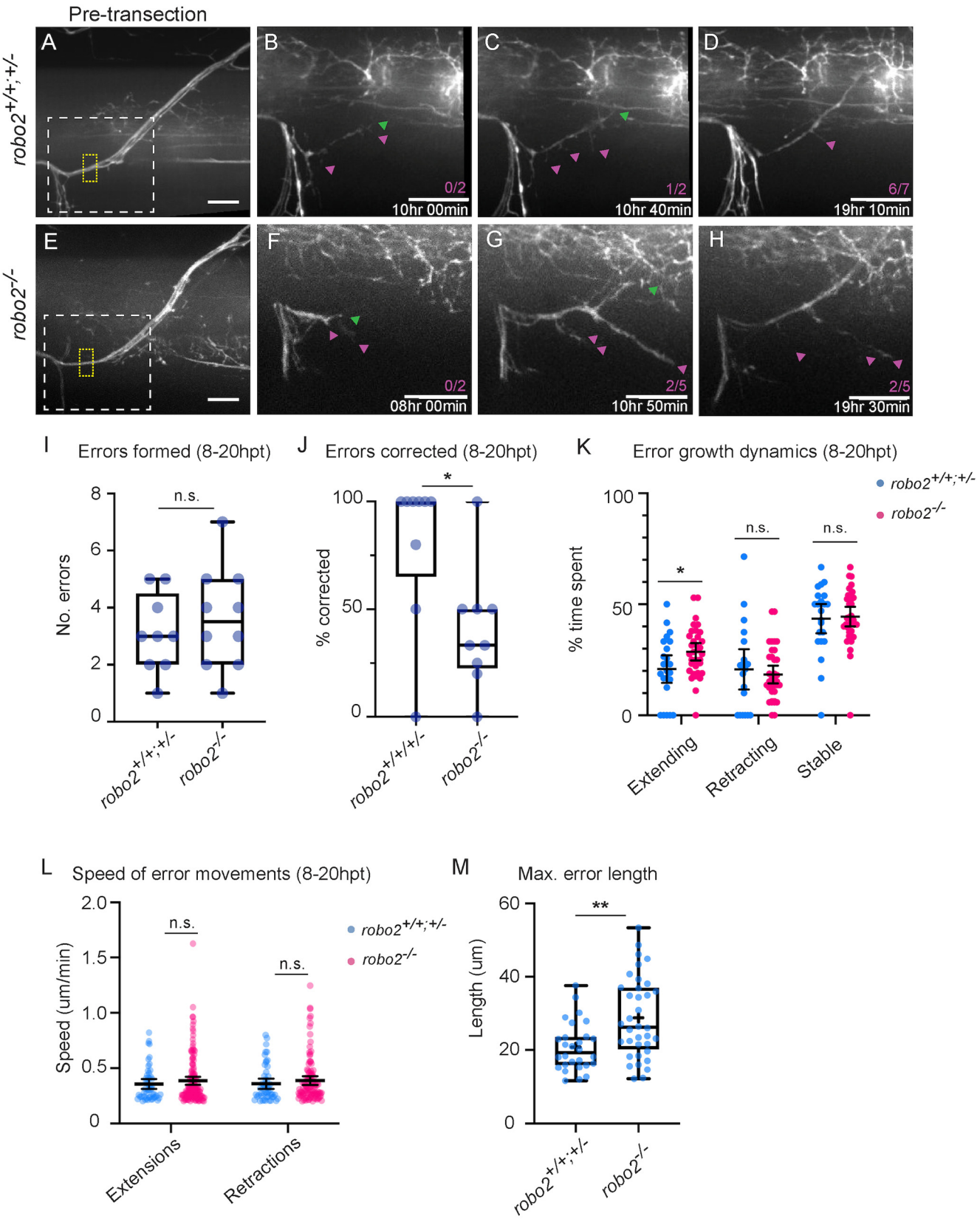

Figure 5. *robo2* prevents error extension at the nerve branch-point during regeneration. Representative images of *Tg(isl1:GFP)* nerves in *robo2*$^{+/-}$ (WT sibling) (***A***) and *robo2*$^{-/-}$ (***E***) at 5 dpf and during regeneration (***B–D***,***F–H***). Dashed yellow box represents transection site. Dashed white box represents area enlarged 2× in ***B–D*** and ***F–H***. Green arrowheads indicate dorsal regrowth. Magenta arrowheads indicate errors. ***B–D***, ***F–H***, Bottom right, White text indicates time after transection. Magenta text counts errors as a fraction of [errors formed/errors corrected]. Scale bars, 10 μm. ***I***, Number of errors formed 8-20 hpt in WT siblings (*robo2*$^{+/+;+/-}$, $n = 9$ nerves) and *robo2*$^{-/-}$ larvae ($n = 10$ nerves). Each dot represents one nerve. Ranks between genotypes were compared using two-tailed Mann–Whitney test ($p = 0.6238$). ***J***, Percent of errors corrected 8-20 hpt in WT siblings (*robo2*$^{+/+;+/-}$, $n = 9$ nerves) and *robo2*$^{-/-}$ larvae ($n = 10$ nerves). Errors were counted as "corrected" when their length measured from the nerve branch-point was <1 μm. Each dot represents one nerve. Ranks were compared between genotypes

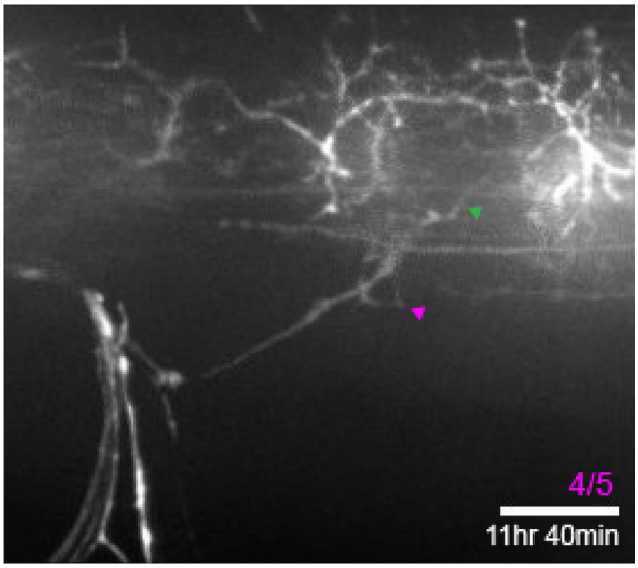

Movie 1. Dorsal nerve fascicle regeneration dynamics in WT sib, related to Figure 3. Representative movie of regenerating axons of dorsal nerve in *robo2*$^{+/-}$ larvae imaged *in vivo* using *Tg(isl1:GFP)*. The movie begins 8 hpt, and images were taken every 10 minutes, as indicated by time counter (white, bottom right), for 12 h. Cumulative error count (magenta, bottom right) is written as a fraction of [number errors corrected number errors formed]. Magenta arrowheads indicate error fascicle movements. Green arrowheads indicate movements of fascicle growing along the dorsal path. Images were processed as described in Materials and Methods. Scale bar, 10 μm. [View online]

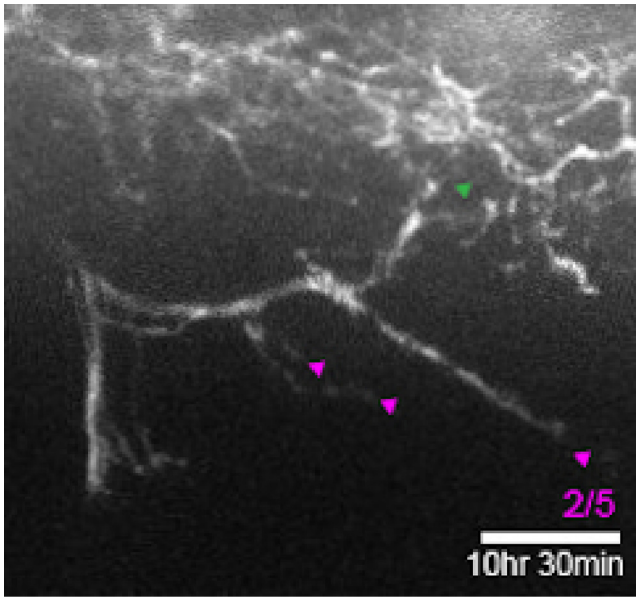

Movie 2. Dorsal nerve fascicle regeneration dynamics in *robo2* mutant, related to Figure 3. Representative movie of regenerating axons of dorsal nerve in *robo2*$^{-/-}$ larvae imaged *in vivo* using *Tg(isl1:GFP)*. The movie begins 8 hpt, and images were taken every 10 minutes, as indicated by time counter (white, bottom right), for 12 h. Cumulative error count (magenta, bottom right) is written as a fraction of [number errors corrected/over number errors formed]. Magenta arrowheads indicate error fascicle movements. Green arrowheads indicate movements of fascicle growing along the dorsal path. Images were processed as described in Materials and Methods. Scale bar, 10 μm. [View online]

exact test). This is consistent with our previous findings that *col4a5* is dispensable for spinal motor nerve development (Isaacman-Beck et al., 2015). Like before, we selected spinal motor nerves with small subsets of mKate^{+} axons along the ventral, but not the dorsal, nerve branch, laser-transected these ventral nerves, and at 48 hpt assessed the regeneration of mKate^{+} axons. Again, we found that, compared with mKate expression, *robo2*-mKate expression in motor neurons did not impair their ability to regrow an axon (for *col4a5*$^{+/+;+/-}$: *Tg(mnx1:mKate; mnx1:mKate)*, $n = 12$ of 24 nerves regenerated by 48 hpt; *Tg(mnx1:mKate; mnx1:robo2)*, $n = 14$ of 21 nerves, $p = 0.3661$, Fisher's exact test; for *col4a5*$^{-/-}$ larvae: *Tg(mnx1:mKate; mnx1:mKate)*, $n = 8$ of 14 nerves; *Tg(mnx1:mKate; mnx1:robo2)*, $n = 9$ of 16 nerves, $p = 0.999$, Fisher's exact test). In *col4a5* siblings and mutants, regenerating ventral nerve axons expressing mKate faithfully selected their original, ventral trajectory (Fig. 7*A*,*B*,*E*,*F*). In *col4a5* siblings, *robo2-mKate* expression was sufficient to redirect regenerating ventral nerve axons onto a dorsal trajectory (Fig. 7*C*,*D*; $p = 0.0425$, Fisher's exact test). In contrast, in *col4a5* mutants, *robo2*-mKate expression failed to redirect ventral nerve axons onto a dorsal trajectory (Fig. 7*G*,*H*), demonstrating that *col4a5* function is required for *robo2* to redirect ventral nerve axons dorsally. This provides compelling evidence that *col4a5* and Slit-Robo act in a common genetic pathway that promotes dorsal branch selection of regenerating axons. Combined, our results support a model in which a small subset of Schwann cells strategically located at the branch choice-point upregulate the expression of *col4a5* and *slit1a* in response to nerve injury. As regenerating axons approach the branch choice-point, Robo2 function selectively in dorsal nerve axons prevents and corrects erroneous projections along ventral and lateral trajectories, thereby biasing axonal regrowth toward their original, dorsal trajectory (Fig. 8).

Discussion

Following peripheral nerve injury, regenerating axons face the challenge of navigating toward and reconnecting with their original synaptic targets. The difficulty of this task increases with the complexity of the injured nerve. After exiting the spinal cord, peripheral nerves repeatedly divide into progressively smaller branches leading to different targets (Lance-Jones and Landmesser, 1981). Regenerating axons may therefore encounter multiple nerve branch-points where they confront the choice to select their appropriate, pre-injury trajectory. Despite this

←

using two-tailed Mann–Whitney test ($p = 0.0208$). ***K***, Quantification of regenerating axon dynamics in WT siblings and *robo2*$^{-/-}$ larvae 8-20 hpt plotted by total time spent extending, retracting, and stable (no movement). Each dot represents one error (for siblings, $n = 23$ errors; for *robo2*$^{-/-}$, $n = 34$ errors). Error movements were examined in 10 min intervals and classified as extensions when there was a ≥ 1 μm increase in error length measured from the MEP; movements were classified as retractions when ≥ 1 μm decrease in error length measured from the MEP; errors were classified as stable when no movement ≥ 1 μm occurred. Line indicates mean. Error bars indicate 95% CIs. Means were compared between genotypes using two-tailed *t* tests (extending, $t_{(55)} = 2.285$, $p = 0.0262$; retracting, $t_{(54)} = 0.5666$, $p = 0.5734$; stable, $t_{(55)} = 0.2540$, $p = 0.8004$). ***L***, Error extension and retraction speed calculated as the absolute value of error movement velocity in micrometers per minute. Extension and retraction events were examined in 10 min intervals and classified as extensions when there was a ≥ 1 μm increase in error length measured from the MEP; movements were classified as retractions when ≥ 1 μm decrease in error length measured from the MEP. Each dot represents one extension or retraction event (for siblings, $n = 23$ errors underwent 51 extension events and 51 retraction events; for *robo2*$^{-/-}$, $n = 34$ errors underwent 139 extension events and 109 retraction events). Line indicates mean. Error bars indicate 95% CIs. Genotypes were compared using two-tailed *t* tests (for extensions, $t_{(188)} = 0.8710$, $p = 0.3849$; for retractions, $t_{(158)} = 0.8706$, $p = 0.3853$). ***M***, Maximum length of errors in WT siblings and *robo2*$^{-/-}$ larvae in micrometers measured from the MEP. Each dot represents one error. +, Mean. Means were compared between genotypes using two-tailed *t* test ($p = 0.0012$). $^{**}p < 0.01$. $^{*}p < 0.05$.

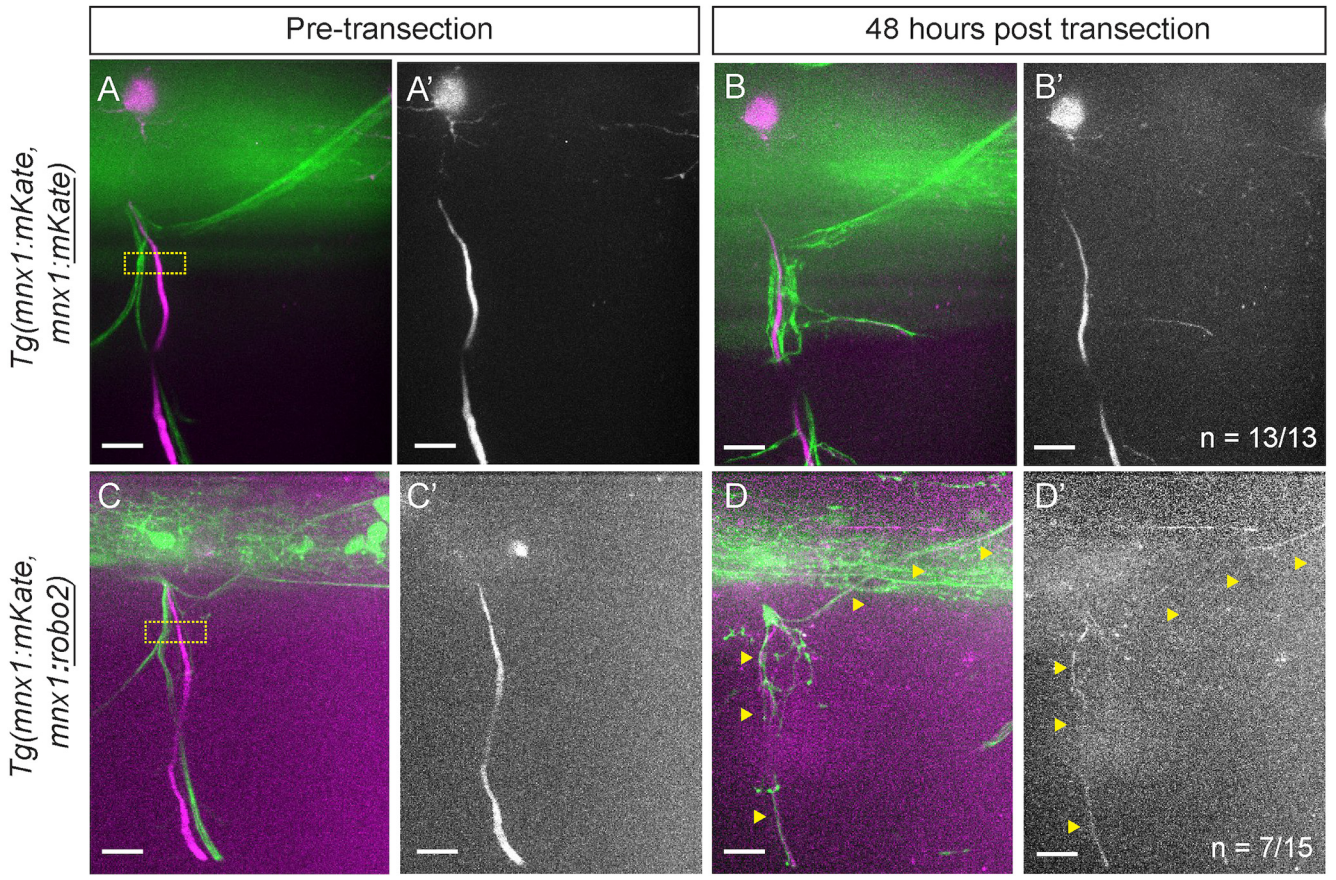

Figure 6. *robo2* is sufficient to promote dorsal branch-selection by regenerating axons. Representative images of *Tg(hb9:GFP)* (green) nerves with small numbers of fascicles expressing transient *Tg(mnx1:mKate, mnx1:mKate)* (***A***,***B***) or *Tg(mnx1:mKate, mnx1:robo2)* (***C***,***D***) (magenta) in small subsets of ventrally projecting motor axons. Merged GFP and mKate images shown at 5 dpf (***A***,***C***) and 48 hpt (***B***,***D***). mKate channel is shown alone at 5 dpf (***A′***,***C′***) and 48 hpt (***B′***,***D′***). In larvae expressing *Tg(mnx1:mKate, mnx1:mKate)*, $n = 13$ of 13 nerves had only ventral regrowth of $mKate^+$ fascicles, as in the example shown. In larvae expressing *Tg(mnx1:mKate, mnx1:robo2)*, $n = 7$ of 15 nerves had dorsal regrowth of $mKate^+$ fascicles, as in the example shown. Proportions of nerves with dorsal regrowth were compared between conditions using one-tailed Fisher's exact test ($p = 0.0054$). Images were processed as described in Materials and Methods. Dashed yellow boxes represent transection site. Scale bars, 10 μm.

enormous navigational challenge, regenerating axons are able to preferentially select their original nerve branch (Politis, 1985; Brushart, 1993; Isaacman-Beck et al., 2015) and regrow toward appropriate targets (Sperry and Arora, 1965; Lundborg et al., 1986; Krarup et al., 2002; Nguyen et al., 2002). Previous studies strongly support the notion that regenerating axons are guided at nerve branch-points by dedicated molecular mechanisms, yet few such mechanisms have been described. Here we identify a molecular pathway critical for communication between glia located at a nerve branch-point and regenerating axons to direct axons of one nerve branch onto their pre-injury trajectory. Specifically, our results provide compelling evidence for transient, spatially restricted, and tightly coordinated signaling events between *col4a5*/*slit1a*-expressing Schwann cells and *robo2*-expressing regenerating axons at a nerve branch-point critical to promote target-selective regeneration.

Robo2 selectively destabilizes erroneous axonal extension at the nerve branch-point

Live cell imaging experiments provide compelling evidence for a Robo2-dependent mechanism that directs regenerating axons into the appropriate nerve branch. As they encounter the nerve branch-point, regenerating dorsal nerve axons in both WT siblings and *robo2* mutants initiate growth (~1 μm) along erroneous ventral and ventrolateral trajectories with similar frequencies (Fig. 5*I*). In *robo2* mutants, axons are more likely to extend along these erroneous trajectories (Fig. 5*K*), ultimately forming errors 1.5-3 times longer than errors observed in WT larvae (Fig. 5*M*). This suggests that (1) *robo2*-independent mechanisms mediate error formation at the nerve branch-point, although it remains to be determined whether this occurs via collateral sprouting, misrouting of entire axons or both; and (2) rather than preventing their initial outgrowth, *robo2* destabilizes axons on erroneous trajectories (> ~1 μm), preventing their further growth. This is markedly different from the role that canonically repulsive axon guidance systems, including Slit-Robo, often play after injury (Hagino et al., 2003; Giger et al., 2010). For example, in *Caenorhabditis elegans*, Slit (*slt-1*) and Robo (*sax-3*) inhibit the extension of the mechanosensory PLM axon after transection, ultimately leading to reduced regeneration (Chen et al., 2011). In contrast, we find identical rates of regenerating axon outgrowth in *robo2* mutants and WT animals (Fig. 5*L*). This provides strong evidence that, during zebrafish peripheral nerve regeneration, *robo2*-independent mechanisms promote axon outgrowth, while *robo2*'s role is to selectively bias regenerative growth of dorsal axons toward their original trajectory.

How similar is this *robo2*-dependent mechanism to other, well-documented mechanisms known to promote target-selective regeneration? In mammals, motor axons preferentially regenerate into their original nerve branches (Mark, 1965; Politis, 1985; Redett et al., 2005). This process is regulated by

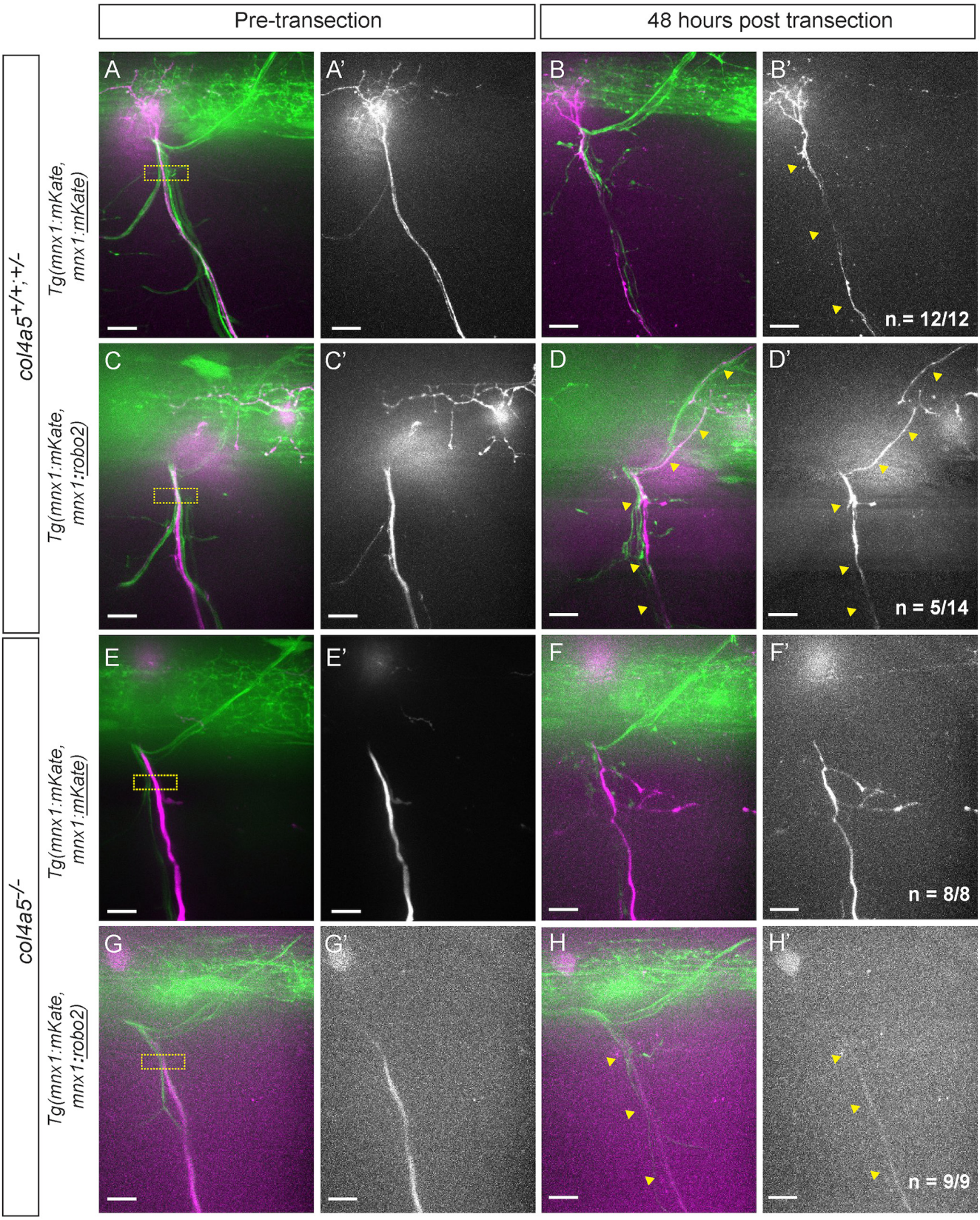

Figure 7. *col4a5* is required for the role of *robo2* in branch-selective axon regeneration. Top, Representative images of *Tg(hb9:GFP)* (green) nerves in col4a5$^{+/-}$ (WT sibling) larvae with fascicles expressing transient *Tg(mnx1:mKate, mnx1:mKate)* (***A***,***B***) or *Tg(mnx1:mKate, mnx1:robo2)* (***C***,***D***) (magenta) in small subsets of ventrally projecting motor axons. Merged GFP and mKate images shown at 5 dpf (***A***,***C***) and 48 hpt (***B***,***D***). mKate channel is shown alone at 5 dpf (***A′***,***C′***) and 48 hpt (***B′***,***D′***). In larvae expressing *Tg(mnx1:mKate, mnx1:mKate)*, $n = 12$ of 12 nerves had only ventral regrowth of mKate^{+} fascicles, as in the example shown. In larvae expressing *Tg(mnx1:mKate, mnx1:robo2)*, $n = 5$ of 14 nerves had dorsal regrowth of mKate^{+} fascicles, as in the example shown. Proportions of nerves with ventral regrowth were compared between conditions using one-tailed Fisher's exact test ($p = 0.0304$). Bottom, Representative images of *Tg(hb9:GFP)* (green) nerves in col4a5$^{-/-}$ larvae with fascicles expressing transient *Tg(mnx1:mKate, mnx1:mKate)* (***E***,***F***) or *Tg(mnx1:mKate, mnx1:robo2)* (***G***,***H***) (magenta) in small subsets of ventrally

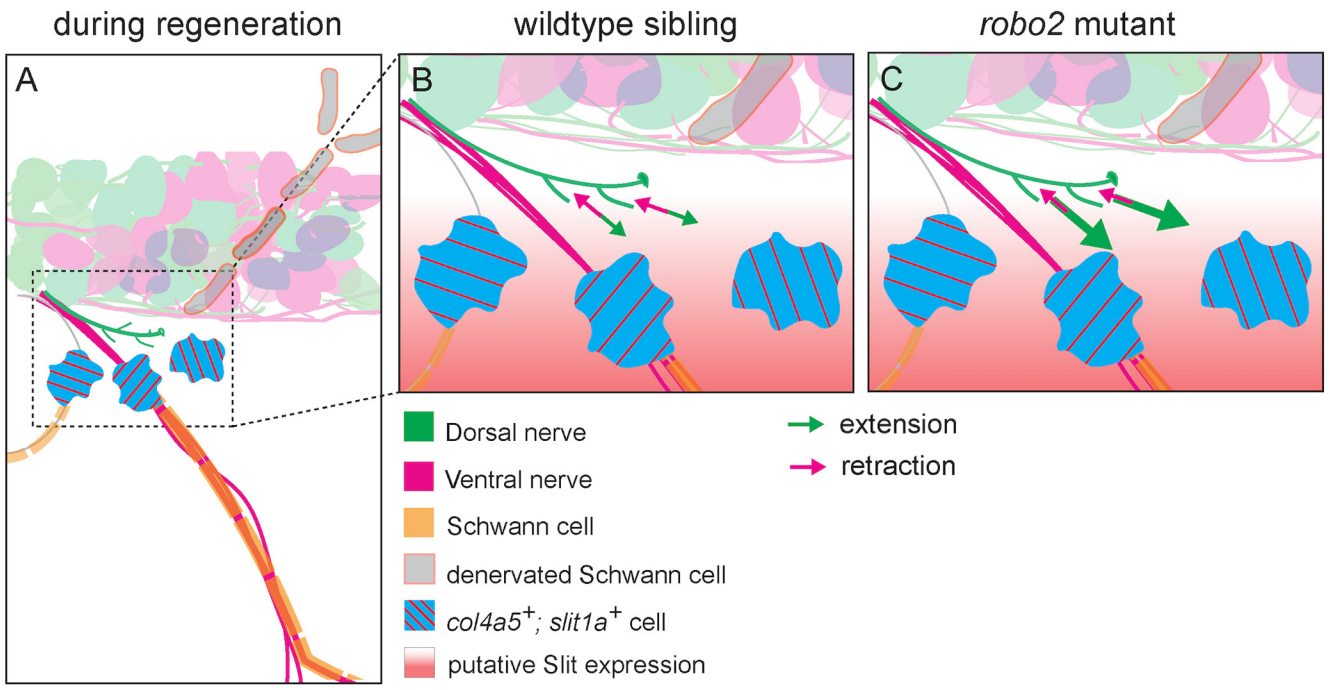

Figure 8. Model for role of *col4a5-robo2* pathway in target-selective axon regeneration. ***A***, During regeneration, a subset of specialized Schwann cells at the nerve branch-point express *col4a5* (blue with red stripes), which scaffolds the repulsive axon guidance cue Slit (red gradient) in the local ECM. ***B***, In response to Slit at the nerve branch-point, regenerating WT axons expressing the Slit-receptor *robo2* extend for short distances along ventral and ventrolateral paths, as they navigate the nerve branch choice-point. These short erroneous extensions (green arrows) are balanced by retraction events (red arrows), which results in their eventual retraction and correction. ***C***, In *robo2*$^{-/-}$ larvae, regenerating axons are not responsive to Slit at the nerve branch-point and thus extend more frequently along ventral and ventrolateral paths. These frequent erroneous extensions (large green arrows) are not balanced by retraction events (red arrows), which occur with similar frequency as retractions in WT siblings. Thus, in *robo2*$^{-/-}$ larvae, branch-point errors extend for longer distances and are less likely to be corrected.

Schwann cells and by nerve end-organs, such as muscle and skin (Madison et al., 2009; Abdullah et al., 2013). For example, after injury, Schwann cells in the distal nerve stump upregulate branch-specific neurotrophic factors and cell adhesion molecules (Höke et al., 2006; Jesuraj et al., 2012; Brushart et al., 2013; Wood and Mackinnon, 2015). These molecules support the outgrowth and maintenance of appropriate axonal populations (Martini et al., 1994; Franz et al., 2005) such that, when axons regenerate into inappropriate nerve branches, the resulting errors are pruned away over weeks or months (Brushart, 1993; Ghalib et al., 2001). Thus, in contrast to well-documented pruning mechanisms that occur long after axons have regenerated toward incorrect targets, the *robo2*-dependent mechanism we describe here is engaged during the time period when regenerating axons confront a choice-point, thereby promoting target-selective regeneration locally and on a much shorter timescale.

A *co4a5*/glia *robo2*/axon-dependent mechanism provides local guidance to promote target-selective regeneration

In response to peripheral nerve injury, Schwann cells distal to the injury site change their differentiation state to that of a repair Schwann cell through a well-characterized molecular pathway (Jessen and Mirsky, 2016, 2019). Repair Schwann cells exhibit location- and modality-specific differences in gene expression (Höke et al., 2006; Jesuraj et al., 2012; Brushart et al., 2013), yet the functional significance of these differences, including their roles in target-selective regeneration, have remained largely unknown. We previously reported that in response to peripheral nerve injury in zebrafish, a small group of Schwann cells (~1-3) located where the dorsal nerve branch deviates from the ventral nerve branch, upregulate *col4a5* and its binding partner, the repulsive guidance cue *slit1a* (Xiao et al., 2011; Isaacman-Beck et al., 2015). While we had shown that *col4a5* is critical for target-selective regeneration, whether the spatial restriction of *col4a5* to just a few Schwann cells was important for target selectivity was unclear. Similarly, whether Slit1a played a functional role in this process and whether Slit1a and *col4a5* expression were functionally related had not been defined.

Our results demonstrate that expanding the expression of *col4a5* to all Schwann cells severely impacts target-selective regeneration (Fig. 1). Although we cannot exclude the possibility that overexpression of *col4a5* affects Schwann cell development, the regeneration phenotype we observe in *Tg(sox10:col4a5-myc)*$^{+}$ larvae is distinct from what we have previously reported in larvae with absent or immature Schwann cells (i.e., mutants for *sox10* or *erbB3*) (see Rosenberg et al., 2014). Rather than extending along random trajectories, regenerating dorsal nerve axons in *Tg(sox10:col4a5-myc)*$^{+}$ larvae extend along erroneous ventral and ventrolateral trajectories, similar to what we observe in mutants lacking *col4a5*, *robo2*, and *extl3*, respectively (Fig. 3) (Isaacman-Beck et al., 2015). Thus, in animals expressing *col4a5* in all Schwann cells, regenerating dorsal nerve axons make errors precisely where they pause and explore the nerve branch-point before turning dorsally during regeneration (Fig. 5). Combined,

←

projecting motor axons. Merged GFP and mKate images shown at 5 dpf (***A***,***C***) and 48 hpt (***B***, ***D***). mKate channel is shown alone at 5 dpf (***E′***,***F′***) and 48 hpt (***G′***,***H′***). In larvae expressing *Tg(mnx1:mKate, mnx1:mKate)*, $n = 8$ of 8 nerves had only ventral regrowth of mKate^{+} fascicles, as in the example shown. In larvae expressing *Tg(mnx1:mKate, mnx1:robo2)*, $n = 9$ of 9 nerves had only ventral regrowth of mKate^{+} fascicles, as in the example shown. Proportions of nerves with ventral regrowth were compared between conditions using one-tailed Fisher's exact test ($p = 0.999$). Dashed yellow boxes represent transection site. Scale bars, 10 μm.

this provides compelling evidence that, rather than providing a permissive substrate and environment, spatially restricted *col4a5* expression is critical to instruct regenerating dorsal nerve axons at the nerve branch-point.

Previous work in rodents and zebrafish has demonstrated that various collagens, including Collagen XV (Guillon et al., 2016), Collagen XIX (Hilario et al., 2010; Wakabayashi, 2021), as well as other ECM components and modifications, play attractive and repulsive roles in axonal development and regeneration (for review, see Chelyshev et al., 2020). Our results highlight a pivotal yet less appreciate role for collagens, not only as an ECM component critical for axonal regeneration, but also as part of an instructive signaling pathway to direct regenerating axons *in vivo*. Indeed, our data provide compelling evidence that precise spatial localization of *col4a5* is critical for its role in peripheral nerve regeneration and suggest a potentially more specialized role for Collagen conduits in clinical applications to direct regenerating peripheral nerve axons toward their original synaptic targets.

Our results also reveal a previously uncharacterized role for Slit-Robo signaling in target-selective regeneration. Loss-of-function mutations in two Slit-Robo signaling components, *extl3* and *robo2*, result in the same target-selective regeneration defects (Fig. 3). Conversely, we find that transgenic expression of *robo2* in ventral nerve axons, which are unaffected by the loss of Slit-Robo signaling, is sufficient to redirect these axons onto a dorsal nerve branch specific route (Fig. 6), and that this process requires *col4a5* (Fig. 7). Given the incomplete penetrance of the *robo2* mutant phenotype in target-selective regeneration, we cannot exclude the possibility that one or multiple of the additional three zebrafish Robo receptors (Lee et al., 2001; Bedell et al., 2005) play a role in this process and hence partially compensate for the loss of *robo2*. Future experiments, including generating single- and double-mutant combinations for the other three Robo receptors as well for each of the four known Slit ligands (Hutson et al., 2003), will provide a comprehensive view on the role of Slit-Robo signaling during target-selective regeneration and inform the contribution of individual Robo receptors in this process.

Nonetheless, our results provide strong support for a mechanism in which glial-derived *col4a5* expression restricted to the branch-point promotes dorsal turning of regenerating axons possibly via Col4a5-bound Slit1a. In the future, it will be important to further characterize the molecular identity of the *col4a5/slit1a*-expressing branch-point Schwann cells, particularly how they sense and respond to spinal motor nerve injury. Candidate regulators of this process include c-Jun and STAT3 (Jessen and Mirsky, 2019), neurotrophic factors (Gordon et al., 2003), and adhesion molecules (Bolívar et al., 2020). The transient expression of *col4a5* and *slit1a*, which lasts only a few hours and coincides with the time period when regenerating axons navigate the branch choice-point is remarkable, underscoring the high degree and functional importance of spatially and temporally coordinated signaling between regenerating axons and Schwann cells to achieve target-selective regeneration. While our results identify a previously uncharacterized molecular mechanism to promote peripheral nerve regeneration, they also draw attention to the need to incorporate spatially and temporally restricted deliveries of guidance information in therapeutic strategies aimed at enhancing target-selective regeneration.

References

Abdullah M, O'Daly A, Vyas A, Rohde C, Brushart TM (2013) Adult motor axons preferentially reinnervate predegenerated muscle nerve. Exp Neurol 249:1–7.

Bedell VM, Yeo SY, Park KW, Chung J, Seth P, Shivalingappa V, Zhao J, Obara T, Sukhatme VP, Drummond IA, Li DY, Ramchandran R (2005) Roundabout4 is essential for angiogenesis in vivo. Proc Natl Acad Sci USA 102:6373–6378.

Blockus H, Chédotal A (2016) Slit-robo signaling. Development 143:3037–3044.

Bolívar S, Navarro X, Udina E (2020) Schwann cell role in selectivity of nerve regeneration. Cells 9:2131.

Bremer J, Granato M (2016) Myosin phosphatase fine-tunes zebrafish motoneuron position during axonogenesis. PLoS Genet 12:e1006440.

Brushart TM (1993) Motor axons preferentially reinnervate motor pathways. J Neurosci 13:2730–2738.

Brushart TM, Aspalter M, Griffin JW, Redett R, Hameed H, Zhou C, Wright M, Vyas A, Höke A (2013) Schwann cell phenotype is regulated by axon modality and central-peripheral location, and persists in vitro. Exp Neurol 247:272–281.

Campbell DS, Stringham SA, Timm A, Xiao T, Law MY, Baier H, Nonet ML, Chien CB (2007) Slit1a inhibits retinal ganglion cell arborization and synaptogenesis via Robo2-dependent and -independent pathways. Neuron 55:231–245.

Chelyshev YA, Kabdesh IM, Mukhamedshina YO (2020) Extracellular matrix in neural plasticity and regeneration. Cell Mol Neurobiol. doi: 10.1007/s10571-020-00986-0.

Chen L, Wang Z, Ghosh-Roy A, Hubert T, Yan D, O'Rourke S, Bowerman B, Wu Z, Jin Y, Chisholm AD (2011) Axon regeneration pathways identified by systematic genetic screening in *C. elegans*. Neuron 71:1043–1057.

Downes GB, Waterbury JA, Granato M (2002) Rapid in vivo labeling of identified zebrafish neurons. Genesis 34:196–202.

Faul F, Erdfelder E, Lang AG, Buchner A (2007) G*Power 3: a flexible statistical power analysis program for the social, behavioral, and biomedical sciences. Behav Res Methods 39:175–191.

Flanagan-Steet H, Fox MA, Meyer D, Sanes JR (2005) Neuromuscular synapses can form in vivo by incorporation of initially aneural postsynaptic specializations. Development 132:4471–4481.

Franz CK, Rutishauser U, Rafuse VF (2005) Polysialylated neural cell adhesion molecule is necessary for selective targeting of regenerating motor neurons. J Neurosci 25:2081–2091.

Fricke C, Lee JS, Geiger-Rudolph S, Bonhoeffer F, Chien CB (2001) Astray, a zebrafish roundabout homolog required for retinal axon guidance. Science 292:507–510.

Ghalib N, Houst'ava L, Haninec P, Dubový P (2001) Morphometric analysis of early regeneration of motor axons through motor and cutaneous nerve grafts. Ann Anat 183:363–368.

Giger RJ, Hollis ER, Tuszynski MH (2010) Guidance molecules in axon regeneration. Cold Spring Harb Perspect Biol 2:a001867.

Gordon T, English AW (2016) Strategies to promote peripheral nerve regeneration: electrical stimulation and/or exercise. Eur J Neurosci 43:336–350.

Gordon T, Sulaiman O, Boyd JG (2003) Experimental strategies to promote functional recovery after peripheral nerve injuries. J Peripher Nerv Syst 8:236–250.

Guillon E, Bretaud S, Ruggiero F (2016) Slow muscle precursors lay down a collagen XV matrix fingerprint to guide motor axon navigation. J Neurosci 36:2663–2676.

Hagino S, Iseki K, Mori T, Zhang Y, Hikake T, Yokoya S, Takeuchi M, Hasimoto H, Kikuchi S, Wanaka A (2003) Slit and glypican-1 mRNAs are coexpressed in the reactive astrocytes of the injured adult brain. Glia 42:130–138.

Hilario JD, Wang C, Beattie CE (2010) Collagen XIXa1 is crucial for motor axon navigation at intermediate targets. Development 137:4261–4269.

Höke A, Redett R, Hameed H, Jari R, Zhou C, Li ZB, Griffin JW, Brushart TM (2006) Schwann cells express motor and sensory phenotypes that regulate axon regeneration. J Neurosci 26:9646–9655.

Hussain SA, Piper M, Fukuhara N, Strochlic L, Cho G, Howitt JA, Ahmed Y, Powell AK, Turnbull JE, Holt CE, Hohenester E (2006) A molecular mechanism for the heparan sulfate dependence of slit-robo signaling. J Biol Chem 281:39693–39698.

Hutson LD, Jurynec MJ, Yeo SY, Okamoto H, Chien CB (2003) Two divergent slit1 genes in zebrafish. Dev Dyn 228:358–369.

Isaacman-Beck J, Schneider V, Franzini-Armstrong C, Granato M (2015) The lh3 glycosyltransferase directs target-selective peripheral nerve regeneration. Neuron 88:691–703.

Jessen KR, Mirsky R (2016) The repair Schwann cell and its function in regenerating nerves. J Physiol 594:3521–3531.
Jessen KR, Mirsky R (2019) The success and failure of the Schwann cell response to nerve injury. Front Cell Neurosci 13:33–14.
Jesuraj NJ, Nguyen PK, Wood MD, Moore AM, Borschel GH, Mackinnon SE, Sakiyama-Elbert SE (2012) Differential gene expression in motor and sensory Schwann cells in the rat femoral nerve. J Neurosci Res 90:96–104.
King AC, Gut M, Zenker AK (2020) Shedding new light on early sex determination in zebrafish. Arch Toxicol 94:4143–4158.
Kosuta C, Daniel K, Johnstone DL, Mongeon K, Ban K, LeBlanc S, MacLeod S, Et-Tahiry K, Ekker M, MacKenzie A, Pena I (2018) High-throughput DNA extraction and genotyping of 3 dpf zebrafish larvae by fin clipping. J Vis Exp 136:58024.
Krarup C, Archibald SJ, Madison RD (2002) Factors that influence peripheral nerve regeneration: an electrophysiological study of the monkey median nerve. Ann Neurol 51:69–81.
Kwan KM, Fujimoto E, Grabher C, Mangum BD, Hardy ME, Campbell DS, Parant JM, Yost HJ, Kanki JP, Chien CB (2007) The Tol2kit: a multisite gateway-based construction Kit for Tol2 transposon transgenesis constructs. Dev Dyn 236:3088–3099.
Lance-Jones C, Landmesser L (1981) Pathway selection by chick lumbosacral motoneurons during normal development. Proc R Soc Lond B Biol Sci 214:1–18.
Lee JS, Ray R, Chien CB (2001) Cloning and expression of three zebrafish roundabout homologs suggest roles in axon guidance and cell migration. Dev Dyn 221:216–230.
Lee JS, von der Hardt S, Rusch MA, Stringer SE, Stickney HL, Talbot WS, Geisler R, Nüsslein-Volhard C, Selleck SB, Chien CB, Roehl H (2004) Axon sorting in the optic tract requires HSPG synthesis by ext2 (dackel) and extl3 (boxer). Neuron 44:947–960.
Lundborg G, Dahlin LB, Danielsen N, Nachemson AK (1986) Tissue specificity in nerve regeneration. Scand J Plast Reconstr Surg 20:279–283.
Madison RD, Sofroniew MV, Robinson GA (2009) Schwann cell influence on motor neuron regeneration accuracy. Neuroscience 163:213–221.
Mark RF (1965) Fin movement after regeneration of neuromuscular connections: an investigation of myotypic specificity. Exp Neurol 12:292–302.
Martini R, Schachner M, Brushart TM (1994) The L2/HNK-1 carbohydrate is preferentially expressed by previously motor axon-associated Schwann cells in reinnervated peripheral nerves. J Neurosci 14:7180–7191.
Mullins MC, Hammerschmidt M, Haffter P, Nüsslein-Volhard C (1994) Large-scale mutagenesis in the zebrafish: in search of genes controlling development in a vertebrate. Curr Biol 4:189–202.
Myers PZ, Eisen JS, Westerfield M (1986) Development and axonal outgrowth of identified motoneurons in the zebrafish. J Neurosci 6:2278–2289.
Nguyen QT, Sanes JR, Lichtman JW (2002) Pre-existing pathways promote precise projection patterns. Nat Neurosci 5:861–867.
Politis MJ (1985) Specificity in mammalian peripheral nerve regeneration at the level of the nerve trunk. Brain Res 328:271–276.
Preibisch S, Saalfeld S, Tomancak P (2009) Globally optimal stitching of tiled 3D microscopic image acquisitions. Bioinformatics 25:1463–1465.
Redett R, Jari R, Crawford T, Chen YG, Rohde C, Brushart TM (2005) Peripheral pathways regulate motoneuron collateral dynamics. J Neurosci 25:9406–9412.
Rosenberg AF, Wolman MA, Franzini-Armstrong C, Granato M (2012) In vivo nerve-macrophage interactions following peripheral nerve injury. J Neurosci 32:3898–3909.
Rosenberg AF, Isaacman-Beck J, Franzini-Armstrong C, Granato M (2014) Schwann cells and deleted in colorectal carcinoma direct regenerating motor axons towards their original path. J Neurosci 34:14668–14681.
Sperry RW, Arora HL (1965) Selectivity in regeneration of the oculomotor nerve in the cichlid fish, *Astronotus ocellatus*. J Embryol Exp Morphol 14:307–317.
Svara FN, Kornfeld J, Denk W, Bollmann JH (2018) Volume EM reconstruction of spinal cord reveals wiring specificity in speed-related motor circuits. Cell Rep 23:2942–2954.
Thisse C, Thisse B (2008) High-resolution in situ hybridization to whole-mount zebrafish embryos. Nat Protoc 3:59–69.
Uemura O, Okada Y, Ando H, Guedj M, Higashijima SI, Shimazaki T, Chino N, Okano H, Okamoto H (2005) Comparative functional genomics revealed conservation and diversification of three enhancers of the isl1 gene for motor and sensory neuron-specific expression. Dev Biol 278:587–606.
van Raamsdonk W, Mos W, Smit-Onel MJ, van der Laarse WJ, Fehres R (1983) The development of the spinal motor column in relation to the myotomal muscle fibers in the zebrafish (*Brachydanio rerio*): I. Posthatching development. Anat Embryol (Berl) 167:125–139.
Wakabayashi T (2021) Transmembrane collagens in neuromuscular development and disorders. Front Mol Neurosci 13:635375.
Westerfield M, McMurray JV, Eisen JS (1986) Identified motoneurons and their innervation of axial muscles in the zebrafish. J Neurosci 6:2267–2277.
Wood MD, Mackinnon SE (2015) Pathways regulating modality-specific axonal regeneration in peripheral nerve. Exp Neurol 265:171–175.
Xiao T, Staub W, Robles E, Gosse NJ, Cole GJ, Baier H (2011) Assembly of lamina-specific neuronal connections by slit bound to type IV collagen. Cell 146:164–176.
Xiao T, Baier H (2007) Lamina-specific axonal projections in the zebrafish tectum require the type IV collagen Dragnet. Nat Neurosci 10:1529–1537.